Inorg. Chem. **2005**, *44*, 6550–6557

Structural and Magnetic Properties of Hexagonal Perovskites $La_{1.2}Sr_{2.7}MO_{7.33}$ (M = Ru, Ir) Containing Peroxide Ions

Thomas Götzfried,* Armin Reller, and Stefan G. Ebbinghaus

Lehrstuhl für Festkörperchemie, Institut für Physik, Universität Augsburg, Universitätsstrasse 1, D-86159 Augsburg, Germany

Received April 5, 2005

The structures of the new compound $La_{1.2}Sr_{2.7}IrO_{7.33}$ and the recently discovered $La_{1.2}Sr_{2.7}RuO_{7.33}$ have been solved using a combination of X-ray and neutron diffraction. Both compounds crystallize in the trigonal space group $R\bar{3}m$ and consist of isolated MO_6 (M = Ru, Ir) octahedra, which are arranged in well-defined hexagonal perovskite slabs. These slabs are separated by ($Sr_2O_{1+\delta}$) layers containing both O^{2-} and $(O_2)^{2-}$ ions. The composition can therefore be written as $La_{1.2}Sr_{2.7}MO_{7-\delta}(O_2)_\delta$ with $\delta = 0.33$. Results of the magnetic susceptibility and XANES measurements show that the transition metal cations are in a pentavalent state. While in $La_{1.2}Sr_{2.7}RuO_{7.33}$ an antiferromagnetic interaction between the Ru^{5+} ions is found, $La_{1.2}Sr_{2.7}IrO_{7.33}$ shows a very small temperature-independent paramagnetism down to 1.8 K due to the strong spin–orbit coupling characteristic for the 5d element iridium.

Introduction

The solid-state chemistry of perovskite-related oxides containing 4d and 5d transition metals has attracted a great deal of attention during the past two decades. Besides demonstrating a wide range of magnetic and electronic properties, these materials show a remarkable compositional flexibility. Many of these oxides possess layered structures consisting of perovskite slabs intergrown with layers of other structural types. Ruddlesden−Popper compounds $A_{n+1}B_nO_{3n+1}$[1,2] or [110]-phases $A_nB_nO_{3n+2}$ (e.g., $Sr_2Nb_2O_7$, $n = 4$[3,4]) are well-known examples consisting of perovskite slabs, the thickness of which is described by the value *n*. These families of compounds have been the subject of many investigations due to their low-dimensional electrical and magnetic properties.

In the class of hexagonal perovskites, the low-dimensional character is even more pronounced. These oxides consist of chains of face-sharing BO_6 octahedra separated by the A cations. Due to the short distance of the B cations (approximately 2.5 Å) direct intermetallic interactions can occur. The BO_6 chains can be interrupted by, e.g., trigonal prisms containing diamagnetic ions. This results in discrete dimers, trimers, etc. of paramagnetic centers, in which interesting coupling phenomena are found.[5,6]

Perovskites generally contain only simple anions such as O^{2-}, N^{3-}, or X^- (X = halogenide). Complex ions cannot easily be incorporated since the perovskite framework consists of (hexagonal or cubic) close-packed (AO_3) layers. In this dense arrangement, only small tetragonal and octahedral vacancies (the latter being partly occupied by the B-type cations) exist, and there is simply not enough space for larger anions. Consequently, the few examples reported belong either to layered derivatives of the perovskite structure, are highly cation deficient, or possess large unit cells. Examples are the carbonate-containing cuprates, like $Sr_2CuO_2(CO_3)$,[7] in which layers of corner-sharing CuO_6 octahedra are connected through carbonate groups. Perovskites containing hydroxide ions often possess the stoichiometry $\square(BB')(OH)_6$; i.e., the A site in these compounds remains unoccupied. The mineral schoenfliesite ($MgSn(OH)_6$) belongs to this group.[8] Finally, an enlargement of

* To whom correspondence should be addressed. E-mail: thomas.goetzfried@physik.uni-augsburg.de.

(1) Rao, C. N. R.; Raveau, B. *Transition Metal Oxides*, 2nd ed.; Wiley-VCH: New York, 1998; p 61.
(2) Sloan, J.; Battle, P. D.; Green, M. A.; Rosseinsky, M. J.; Vente, J. F. *J. Solid State Chem.* **1998**, *138*, 135.
(3) Scheunemann, K.; Müller-Buschbaum, H. K. *J. Inorg. Nucl. Chem.* **1975**, *37*, 1679.
(4) Lichtenberg, F.; Herrnberger, A.; Wiedenmann, K.; Mannhart, J. *Prog. Solid State Chem.* **2001**, *29*, 1.
(5) Lightfoot, P.; Battle, P. *J. Solid State Chem.* **1990**, *89*, 174.
(6) Cussen, E. J.; Vente, J. F.; Battle, P. D. *J. Am. Chem. Soc.* **1999**, *121*, 3958.
(7) Narendra Babu, T. G.; Fish, D. J.; Greaves, C. *J. Mater. Chem.* **1991**, *1*, 677.
(8) Strunz, H.; Contag, B. *Acta Crystallogr.* **1960**, *13*, 601.

10.1021/ic050511s CCC: $30.25
Published on Web 08/25/2005

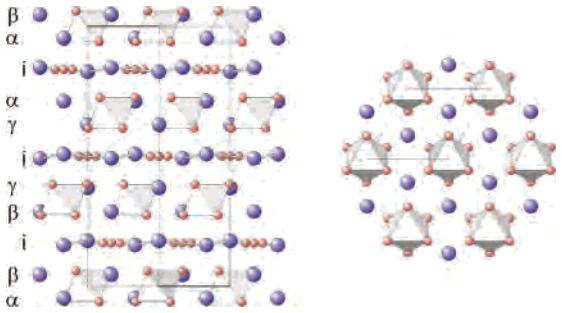

Figure 1. Left: Projection of the crystal structure of $La_{1.2}Sr_{2.7}MO_{7+\delta}$ (M = Ru, Ir) along the (110) direction; greek letters represent the (AO_3) layers (A = La/Sr), i the intermediate ($A'_2O_{1+\delta}$) layers (A′ = Sr). The transition metal cations are located in the octahedra. Right: Hexagonal perovskite layer $(La,Sr)_2MO_6$ (M = Ru, Ir) viewed down the *c*-direction.

the unit cell allows the formation of $Cs_2LiCr(CN)_6$, which can be described as a double perovskite with oxygen replaced by CN^- ions.[9] While the oxidic double perovskites have unit cells of about 8 Å, in this compound the cell parameter is increased to approximately 10 Å.

Besides the academic interest these materials generate, perovskites containing complex anions may also serve as functional materials. Changes in the anion stoichiometry are known to strongly alter the physical properties of a huge variety of perovskites. For this reason, compounds with complex anions might become interesting as sensor materials, provided that the corresponding anion can reversibly be exchanged.

Against this background, the discovery of perovskites containing peroxide ions was rather astonishing.[10] To the best of our knowledge, all known peroxide-containing perovskites belong to one family having the general composition $(A'_2O_{1+\delta})(A_nB_{n-1}O_{3n})$.

Very few representatives belonging to this family have been reported to date: one example is the system $Ba_5Ru_2O_{10}/Ba_5Ru_2O_9(O_2)$[10,11] corresponding to $n = 3$ with $\delta = 0$ and 1, respectively. While $\delta = 0$ describes a simple oxidic material, for $\delta = 1$ the two oxygens in the ($A'_2O_{1+\delta}$) layers form peroxide units (O_2^{2-}). This particular feature is also found in the system $Ln_2Ca_2MnO_{7+\delta}$,[12−14] an $n = 2$ member of this series. In a recent article, we reported on the new 4d transition metal oxide $La_{1.2}Sr_{2.7}RuO_{7+\delta}$.[15] Structural investigations based on X-ray diffraction data showed $La_{1.2}Sr_{2.7}RuO_{7+\delta}$ to be isostructural to $La_2Ca_2MnO_{7+\delta}$. Figure 1 (left) represents the $n = 2$ crystal structure viewed along the (110) direction. The structure can be described by the stacking of close-packed (AO_3) layers, according to the sequence $\alpha\beta\beta\gamma\gamma\alpha$..., divided by one intermediate ($A'_2O_{1+\delta}$) layer (i) to give the stacking sequence $\alpha\beta i\beta\gamma i\gamma\alpha$... The transition metal cations occupy the octahedral interstitial sites between neighboring (AO_3) layers resulting in the formation of hexagonal perovskite-related A_2BO_6 slabs. In this arrangement, the B-type cations form isolated octahedra separated by ($A'_2O_{1+\delta}$) layers along the *c*-axis. Figure 1 (right) illustrates one of these octahedron layers reflecting the trigonal symmetry. For $La_{1.2}Sr_{2.7}RuO_{7+\delta}$, XRD-Rietveld refinements together with thermogravimetric measurements led to a value of $\delta \approx 1/3$ and revealed the presence of both oxide and peroxide ions in the ($A'_2O_{1+\delta}$) layers.

In a systematic study to replace ruthenium by other noble metals, we managed to prepare the new compound $La_{1.2}Sr_{2.7}IrO_{7.33}$ which turned out to be the Ir-analogue of the above-mentioned ruthenate. $La_{1.2}Sr_{2.7}IrO_{7.33}$ is the first $n = 2$ oxide of the $(A'_2O_{1+}\delta)(A_nB_{n-1}O_{3n})$ series containing a 5d transition metal. The only other iridium-containing member of this series known to date is $Ba_{3.44}K_{1.56}Ir_2O_{10}$ ($n = 3$, $\delta = 0$).[16]

In this Article, we report structural, magnetic, and electronic properties of the new iridate determined by combined X-ray and neutron powder diffraction, by measurements of the magnetic susceptibility and X-ray absorption spectroscopy, respectively. Comparing the results with the corresponding ruthenate reveals a high structural similarity but a dramatic change of the physical properties with the replacement of the 4d by a 5d transition metal.

Experimental Section

Polycrystalline samples of $La_{1.2}Sr_{2.7}MO_{7.33}$ (M = Ru, Ir) were prepared by heating appropriate amounts of decarbonated La_2O_3, $SrCO_3$, RuO_2, and Ir metal, respectively, in air at 1250 °C for 36 h. The products were slowly cooled to 900 °C within 35 h, after which the furnace was switched off. The obtained powders were of reddish-brown and black color for the ruthenate and iridate, respectively.

X-ray powder diffraction measurements were carried out on a Seifert 3003-TT diffractometer in the range $13° \le 2\theta \le 120°$ with a step width of 0.015° and a measuring time of 10 s per data point using Cu Kα radiation.

The neutron powder diffraction patterns were recorded on the high-resolution powder diffractometer for thermal neutrons (HRPT)[17] at PSI, Villigen (Switzerland). The samples (about 3 g) were enclosed in a cylindrical vanadium container of 8 mm inner diameter. Data collection was performed at room temperature with the following experimental conditions: $\lambda = 1.494$ Å, 2θ range 5−165°, 2θ step size 0.05°.

A simultaneous Rietveld refinement of the XRD and ND data was performed with FullProf2k Multi-Pattern.[18] For the neutron data, a Thompson−Cox−Hastings pseudo-Voigt peak-shape function was used, whereas the X-ray data were fitted with a pseudo-Voigt function. The background of each data set was described by interpolation between a set of fixed points. The neutron patterns, which were recorded in transmission mode, were absorption-corrected. The calculated absorption correction coefficient (μR) was

(9) Ryan, R. R.; Swanson, B. I. *Inorg. Chem.* **1974**, *13*, 1681.
(10) Grasset, F.; Dussarrat, C.; Darriet, J. *J. Mater. Chem.* **1997**, *7*, 1911.
(11) Dussarrat, C.; Fompeyrine, J.; Darriet, J. *Eur. J. Solid State Inorg. Chem.* **1994**, *31*, 289.
(12) Wang, Y.; Lin, J.; Du, Y.; Qin, R.; Han, B.; Loong, C. K. *Angew. Chem., Int. Ed.* **2000**, *39*, 2730.
(13) Gaudin, E.; Goglio, G.; Besnard, A.; Darriet, J. *J. Solid State Chem.* **2003**, *175*, 124.
(14) Wang, Y.-X.; Bie, L.-J.; Du, Y.; Lin, J. H.; Loong, C.-K.; Richardson, J. W., Jr.; You, L.-P. *J. Solid State Chem.* **2004**, *177*, 65.
(15) Götzfried, T.; Reller, A.; Ebbinghaus, S. G. *Solid State Sci.* **2004**, *6*, 1205.
(16) Kim, S.-J.; Smith, M. D.; Darriet, J.; zur Loye, H.-C. *J. Solid State Chem.* **2004**, *177*, 1493.
(17) Fischer, P.; Frey, G.; Koch, M.; Könnecke, M.; Pomjakushin, V.; Schefer, J.; Thut, R.; Schlumpf, N.; Bürge, R.; Greuter, U.; Bondt, S.; Berruyer, E. *Physica B* **2000**, *276*, 146.
(18) Rodriguez-Carvajal, J. *PROGRAM FullProf.2k (Version 2.40 − May 2003 − ILL)*.

found to be 0.1 for $La_{1.2}Sr_{2.7}RuO_{7.33}$, whereas for the iridium-containing compound a value of 2.0 was obtained.

Peaks caused by the vanadium container were excluded from the diffraction pattern, and a trace impurity of $La(OH)_3$ was included in the refinements of the XRD data. A quantitative analysis revealed that the fraction of this phase was well below 1% for the two title compounds.

The total oxygen content was determined by thermogravimetric analysis (TGA) in a Netzsch STA 409C thermobalance using 5% H_2/N_2 as reducing agent. About 50 mg of sample was heated to 1200 °C at a rate of 10 °C min^{-1} and a gas flow of 70 mL min^{-1}.

The temperature dependence of the magnetic susceptibility was investigated using a Quantum Design MPMS SQUID magnetometer. Samples were measured under both zero-field cooled (ZFC) and field cooled (FC) conditions in the temperature range $1.8 \leq T \leq 300$ K.

X-ray absorption experiments at the Ir-L_{III} edge were carried out at the beamline A1 of HASYLAB at DESY. XANES spectra of the iridate and several reference materials were recorded in transmission mode at room temperature. Appropriate amounts of the samples were mixed with polyethylene and pressed into pellets to obtain an edge step $\Delta\mu d \sim 1-2$. Reproducibility of the determination of the edge position was achieved by recording spectra of a Pt metal foil before and after each measurement of a series of compounds. The obtained raw data were energy calibrated, background corrected (Victoreen fit), and normalized.

Results and Discussion

To examine the compositional range of the desired ruthenate phase, a systematic study on possible stoichiometries was performed, assuming a total of four A-type cations. Therefore, the La/Sr ratio was varied, independent of the possible oxidation state of the transition metal. For ratios La/Sr = 1:3 and 1.1:2.9, respectively, the X-ray diffraction (XRD) revealed additional peaks corresponding to the Sr_2MO_4 phase. A higher La content, for example La/Sr = 1.3:2.7, on the other hand, led to a La_2O_3 impurity. Only for La/Sr = 1.2:2.8 was the synthesized compound found to be single-phase in the XRD. The same composition was used for the preparation of the iridate. However, refinement calculations (vide infra) revealed that the compound was in fact slightly A′ cation deficient.

Rietveld Structure Refinement. A structural model for $La_{1.2}Sr_{2.7}RuO_{7+\delta}$ achieved by XRD-Rietveld refinement has been reported recently.[15] In this paper, we present joint refinements of X-ray and neutron diffraction data for the ruthenate and the new isostructural iridate. These joint refinements provide a much deeper insight in some structural aspects. Due to the high neutron scattering length of oxygen, detailed information about the oxygen stoichiometry as well as metal−O bond lengths, angles, and (anisotropic) displacement parameters can be derived. Figure 2 shows the profile fits to the neutron and X-ray diffraction data, respectively, for both title compounds. Refinement results are given in Table 1, and selected interatomic distances are listed in Table 2.

The La1/Sr1 position was refined by constraining the site to be fully occupied, and only the La/Sr ratio was allowed to vary. For the trigonal prismatically coordinated A′ cations, on the other hand, a refinement with the cations occupying

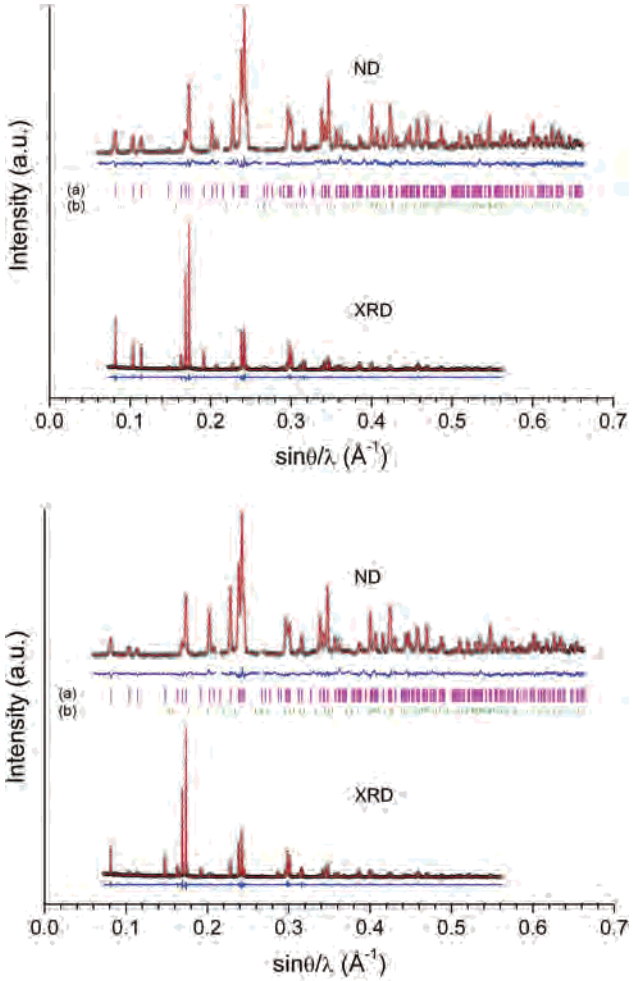

Figure 2. Observed (○), calculated (−), and difference (bottom) X-ray and neutron powder diffraction patterns for $La_{1.2}Sr_{2.7}IrO_{7.33}$ (top) and $La_{1.2}Sr_{2.7}RuO_{7.33}$ (bottom). Bragg reflections for the respective compound (a) and $La(OH)_3$ (b) are represented by tick marks.

the (0,0,*z*) position only led to very large and strongly oblate displacement parameter. Difference Fourier calculations revealed a high remaining electron density at (2*x*,*x*,*z*) with $x \approx 0.05$. Positioning the A′ cations on this site, however, resulted in a high difference peak at (0,0,*z*). For this reason, a split model was applied with one part of the ions positioned on the *c*-axis and an additional part occupying the 18*h* off-center position close to this axis. Positioning both lanthanum and strontium on these sites led to negative occupancy parameters for lanthanum. This indicates that the trigonal prisms are occupied by strontium ions only. It is to be noted that the sum of the occupancy parameters for these sites, i.e., Sr2 and Sr2a, yields a 90% occupation consistent with the slightly cation-deficient composition. A deficiency for the A′ cations in combination with a partial disorder seems to be typical for the $(A'_2O_{1+\delta})(A_nB_{n-1}O_{3n})$ hexagonal perovskites. A very similar situation was already observed in the $n = 3$ member $Ba_{4.9}Ru_2O_{10.8}$.[10]

The most interesting structural feature of the title compounds concerns the oxygen position within the $(A'_2O_{1+\delta})$ layers. The oxygen ions do not occupy the 3*b* site, i.e., the center of the hexagonal cavity formed by the A′ ions, but are delocalized on an off-center position. In previous

Table 1. Atomic Coordinates Refined with X-ray and Neutron Diffraction Data of $La_{1.2}Sr_{2.7}MO_{7+\delta}$ (M = Ru, Ir) at Room Temperature

atom	site	SOF	*x*	*y*	*z*	B_{eq} (Å^2)
		$La_{1.2}Sr_{2.7}RuO_{7+\delta}$				
$\delta = 0.31(3)$ (from Rietveld refinement), $\delta = 0.35(3)$ (from TGA)						
space group $R\bar{3}m$, $a = 5.753(1)$ Å, $c = 18.351(3)$ Å, $V = 526.05(2)$ Å^3, $Z = 3$, calcd density 8.110 g/cm^3						
X-ray data: $R_p = 0.0820$, $R_{wp} = 0.110$						
neutron data: $R_p = 0.0308$, $R_{wp} = 0.0399$						
Ru	3*a*	1	0	0	0	0.619(37)
La1/Sr1	6*c*	0.578(15)/ 0.422(15)	0	0	0.62326(7)	0.904(30)
Sr2	6*c*	0.709(20)	0	0	0.1753(2)	0.72(8)
Sr2a	18*h*	0.065(6)	0.099(5)	0.050(5)	0.1744(9)	0.72(8)
O1	18*h*	1	0.3157(4)	0.1576(4)	0.0611(1)	3.562[a]
O2a	18*g*	0.158(10)	0.1155(15)	0	0.5	0.74(18)
O2b	18*h*	0.061(9)	0.092(9)	0.185(9)	0.5	0.74(18)
		$La_{1.2}Sr_{2.7}IrO_{7+\delta}$				
$\delta = 0.35(3)$ (from Rietveld refinement), $\delta = 0.41(3)$ (from TGA)						
space group $R\bar{3}m$, $a = 5.771(1)$ Å, $c = 18.348(3)$ Å, $V = 529.13(2)$ Å^3, $Z = 3$, calcd density 8.362 g/cm^3						
X-ray data: $R_p = 0.0820$, $R_{wp} = 0.112$						
neutron data: $R_p = 0.0338$, $R_{wp} = 0.0438$						
Ir	3*a*	1	0	0	0	0.767(29)
La1/Sr1	6*c*	0.557(12)/ 0.443(12)	0	0	0.62293(7)	0.947(36)
Sr2	6*c*	0.788(16)	0	0	0.1753(1)	1.03(9)
Sr2a	18*h*	0.047(5)	0.123(7)	0.062(7)	0.1717(14)	1.03(9)
O1	18*h*	1	0.3194(5)	0.1595(5)	0.0616(1)	3.581[b]
O2a	18*g*	0.165(11)	0.1157(19)	0	0.5	0.80(21)
O2b	18*h*	0.064(11)	0.093(10)	0.19(10)	0.5	0.80(21)

[a] Refined with the following anisotropic displacement parameters (Å^2): $\beta_{11} = 2\beta_{12}$, $\beta_{22} = 0.0654(10)$, $\beta_{33} = 0.0011(1)$, $\beta_{12} = 0.0039(7)$, $\beta_{13} = 2\beta_{23}$, $\beta_{23} = -0.0001(1)$. [b] Refined with the following anisotropic displacement parameters (Å^2): $\beta_{11} = 2\beta_{12}$, $\beta_{22} = 0.0625(11)$, $\beta_{33} = 0.0013(1)$, $\beta_{12} = 0.0046(8)$, $\beta_{13} = 2\beta_{23}$, $\beta_{23} = -0.0002(2)$.

Table 2. Selected Bond Lengths (Å)

	$La_{1.2}Sr_{2.7}RuO_{7+\delta}$	$La_{1.2}Sr_{2.7}IrO_{7+\delta}$
6 × Ru−O1	1.932(2)	
6 × Ir−O1		1.957(3)
3 × La1/Sr1−O1	2.596(2)	2.599(3)
6 × La1/Sr1−O1	2.896(2)	2.904(3)
1 × La1/Sr1−O2a	2.358(2)	2.354(3)
1 × La1/Sr1−O2b	2.443(17)	2.443(20)
3 × Sr2−O1	2.496(3)	2.480(3)
3 × Sr2−O1	2.620(3)	2.628(3)
1 × Sr2a−O1[a]	2.191(24)	2.151(33)
1 × Sr2a−O1[a]	2.342(22)	2.247(31)
1 × Sr2−O2a[b]	2.772(7)	2.779(8)
1 × Sr2−O2b[b]	2.407(56)	2.404(64)

[a] Only shortest distance to strontium ion occupying 3-fold degenerate site 18*h*. [b] Only shortest distance to oxygen ion occupying 6-fold degenerate site 18*g* (O2a)/18*h* (O2b).

reports,[13,14,19] refinements were carried out with oxygen occupying the 18*g* (x,0,$^1/_2$) site only. However, difference Fourier analysis without the O2 showed a toroid-shaped residual density without clear peaks at this position. Therefore, the oxygen ions were allowed to occupy both the 18*g* and the intermediate 18*h* site (x,2x,z), with z being fixed to $^1/_2$. Identical displacement parameters were used for these sites, whereas the occupancies were refined independently. It turned out that the 18*g* site is indeed preferably occupied, consistent with previous results. From the site occupation factors (SOFs) given in Table 1, a total oxygen content of 7.35(3) for the iridate and 7.31(3) for the ruthenate is obtained. These values are in good agreement with the thermogravimetric results. Heating the samples to 1200 °C in a reducing atmosphere of 5% H_2/N_2 resulted in the formation of iridium (ruthenium) metal, La_2O_3, SrO, and gaseous H_2O, which was identified by mass spectroscopy. From the obtained weight loss of 6.83% for the iridiate (7.34% for the ruthenate[15]), a total oxygen content of 7.41 for the iridate (7.35 for the ruthenate) is deduced. The estimated standard deviations for these values can be approximated to be 0.03. Since the thermogravimetric results may be biased by the presence of (amorphous) trace impurities, we believe that the values achieved by neutron diffraction are more reliable. Within the experimental error, δ is 0.33 for both the iridate and the ruthenate. For this reason, the slightly idealized notation $La_{1.2}Sr_{2.7}MO_{6.67}(O_2)_{0.33}$ will be used henceforth in this article.

Following the discussion in ref 15, δ values larger than 0 can only be explained by the presence of peroxide ions within the ($A'_2O_{1+\delta}$) layers. Please note that in this notation δ is identical to the number of peroxide ions, while the number of oxide ions in this layer is given by ($1 - \delta$). The replacement of O^{2-} (oxide ion) by $(O_2)^{2-}$ (peroxide ion) does not change the oxidation state of the transition metal ion.

Since our refinements revealed the presence of oxygen both on the 18*g* and 18*h* sites within the ($A'_2O_{1+\delta}$) layers, the question arises which of these positions is occupied by the peroxide ions. A survey of the ICSD (inorganic crystal structure database) yielded typical O−O bond lengths of roughly 1.5 Å for the peroxide ion. After looking at the values given in Figure 3, it is obvious that the distances between the 18*g* and 18*h* site best match this value. The obtained O−O bond lengths of 1.549(26) Å for the iridate and 1.533(28) Å for the ruthenate are in good agreement with the distance of 1.554 Å reported for $Ba_5Ru_2O_{11}$.[10] Using the SOFs listed in Table 1, the asymmetric arrangement of the peroxide unit involving both the 18*h* and 18*g* site (with the O^{2-} ions occupying only the 18*g* positions as described in refs 13,14, and19) leads to a δ value of 0.38(7)

(19) Ebbinghaus, S. G. *J. Solid State Chem.* **2004**, *177*, 817.

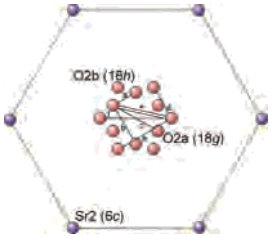

Figure 3. View of the ($A'_2O_{1+\delta}$) layer of $La_{1.2}Sr_{2.7}MO_{7.33}$ perpendicular to the *c*-axis. Distances (in Å) between oxygen atoms are (a) 0.665/0.668, (b) 1.151/1.157, (c) 1.329/1.336, (d) 0.921/0.934, (e) 1.595/1.618, and (f) 1.842/1.868 for M = Ru/Ir. The asterisk indicates the position of one peroxide unit with a bond length of 1.533 and 1.549 Å for $La_{1.2}Sr_{2.7}RuO_{7.33}$ and $La_{1.2}Sr_{2.7}IrO_{7.33}$, respectively.

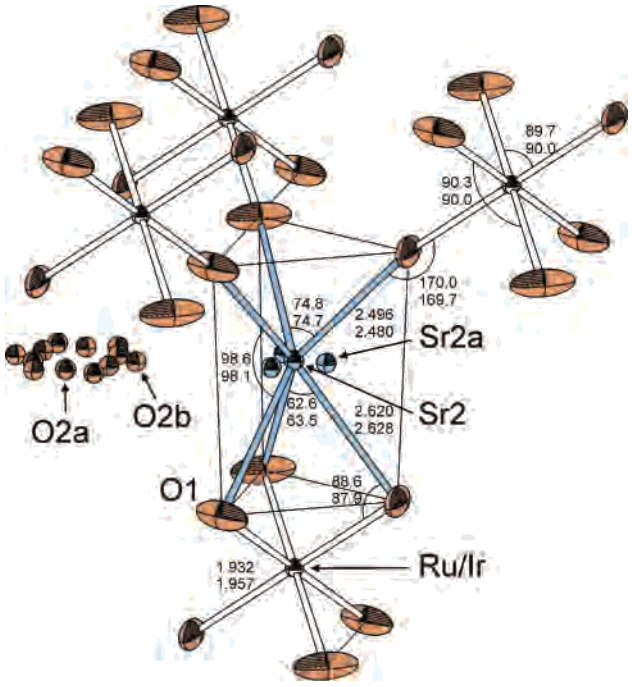

Figure 4. Detailed view of the crystal structure showing the connection between triangular SrO_6 prisms and MO_6 octahedra as well as selected bond lengths (Å) in $La_{1.2}Sr_{2.7}MO_{7.33}$ with M being Ru (upper numbers) and Ir (lower numbers), respectively. Displacement ellipsoids are drawn at the 50% probability level.

for the iridate and 0.37(5) for the ruthenate. These values are within experimental error identical to the composition $La_{1.2}Sr_{2.7}MO_{6.67}(O_2)_{0.33}$ derived above.

The displacement ellipsoids for the oxygen ions on the O1 site were found to be rather elongated (Figure 4), indicating that the anions either are thermally mobile or possess a considerable positional disorder. To distinguish dynamic from static disorder, refinement calculations were carried out on neutron diffraction data collected at 1.5 K. Since the neutron scattering lengths of lanthanum and strontium are similar (8.24 and 7.02 fm, respectively), the La1/Sr1 ratio was fixed to the SOFs derived from the XRD data at room temperature. The refinement results show that the anisotropic displacement parameters for the O1 site are comparable to those obtained from joint refinement at room temperature, favoring a static disorder of these ions.

Comparison of the Structures. For both compounds, the BO_6 octahedra maintain an almost perfect O_h symmetry with O−M−O bond angles close to 90°. The experimentally

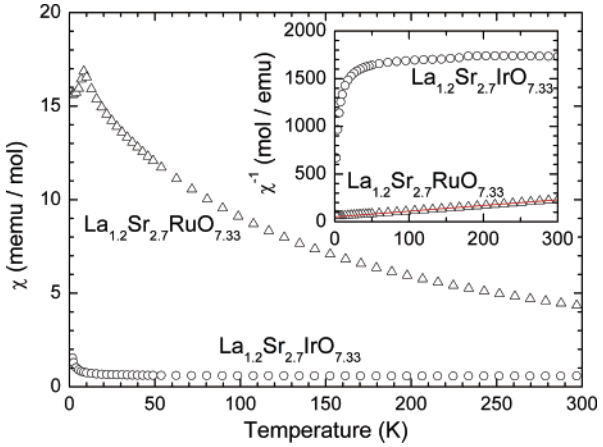

Figure 5. Temperature dependence of the molar magnetic susceptibilities measured in an applied field of 20 kG for $La_{1.2}Sr_{2.7}IrO_{7.33}$ and $La_{1.2}Sr_{2.7}RuO_{7.33}$. In the inset, the inverse susceptibilities are shown. For the ruthenate, the fitted Curie−Weiss law is displayed.

found B−O bond lengths are 1.932(2) and 1.957(3) Å for the ruthenate and iridate, respectively. The electron density of the O1 positions is modeled as an ellipsoid (see Figure 4). This leads to an artificial bond shortening; i.e., the determined atomic distances are shorter than the real bond lengths. Nevertheless, the experimental results can be compared with the values deduced from bond valence sum calculations using the method of Brown and Altermatt.[20] Since magnetic and XANES results (vide infra) yield an oxidation state of +5 for the transition metal cations, the bond valence parameters 1.888 Å[21] and 1.916 Å[22] for Ru^{5+} and Ir^{5+}, respectively, were used in the calculations. For the Ru−O bond length a value of 1.955 Å is expected, whereas the distance in the iridate is calculated to be 1.983 Å. These distances are about 0.02 Å longer than the experimentally determined ones, a finding consistent with the above-mentioned artificial bond shortening.

Magnetic Measurements. Recent magnetic investigations on $La_{1.2}Sr_{2.7}RuO_{7.33}$ indicated the presence of an antiferromagnetic interaction between the ruthenium centers associated with the occurrence of a long-range antiferromagnetic ordering at low temperatures. Owing to the close structural similarity, one would also expect antiferromagnetic coupling for the iridate. A comparison of the magnetic susceptibilities of $La_{1.2}Sr_{2.7}RuO_{7.33}$ and $La_{1.2}Sr_{2.7}IrO_{7.33}$ in an applied field of 20 kG is shown in Figure 5. The data for the ruthenate reveal an antiferromagnetic transition at 7 K consistent with previous results, whereas the susceptibility of the iridate proves that this compound is paramagnetic down to 1.8 K without any magnetic ordering. For both compounds, the ZFC and FC (for clarity not shown in the figure) data completely overlay at all temperatures except for a minimal deviation at the very lowest temperatures measured. The inverse susceptibility of $La_{1.2}Sr_{2.7}IrO_{7.33}$ (inset of Figure 5) clearly demonstrates that, unlike the ruthenate, no Curie−Weiss behavior is observed. The explanation for this unusual

(20) Brown, I. D.; Altermatt, D. *Acta Crystallogr., Sect. B* **1985**, *41*, 244.
(21) Dussarrat, C.; Grasset, F.; Bontchev, R.; Darriet, J. *J. Alloys Compd.* **1996**, *233*, 15.
(22) Brese, N. E.; O'Keefe, M. *Acta Crystallogr., Sect. B* **1991**, *47*, 192.

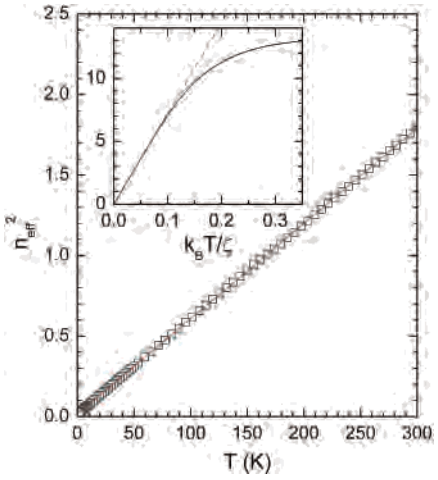

Figure 6. Temperature dependence of the square of the effective magneton number for $La_{1.2}Sr_{2.7}IrO_{7.33}$ and the corresponding linear fit. The inset shows n_{eff}^2 versus k_BT/ζ according to Kotani's formula for $^3T_1$ terms and the linear behavior (---) for $k_BT \ll \zeta$.

magnetic behavior of $La_{1.2}Sr_{2.7}IrO_{7.33}$ results from the strong spin−orbit coupling observed in the 5d transition metals.[23] From the XANES measurements discussed below, the valence of Ir was found to be +5. Due to the strong crystal field splitting in the 5d series, the Ir^{5+} ions have a low-spin configuration ($t_{2g}^4e_g^0$). The resulting ground term in an octahedral crystal field is $^3T_{1g}$. For T terms, a reduced orbital angular momentum of $L' = 1$ remains, which couples with the spin of $S = 1$ giving rise to three energy eigenstates with $J = 0,1$, and 2. According to Kotani's theory on the magnetic moment of complex ions,[24] the effective magnetic moment depends on the thermal population of these states, which is expressed as the ratio of temperature (k_BT) to spin−orbit coupling constant (ζ) as follows:

$$n_{\text{eff}}^2 = \frac{3}{2}y \cdot \frac{24 + (1/y - 9)\exp(-1/y) + (5/y - 15)\exp(-3/y)}{1 + 3\exp(-1/y) + 5\exp(-3/y)}$$

with

$$y \equiv \frac{2k_BT}{\zeta}$$

This behavior is displayed in the inset of Figure 6. For Ir^{5+}, the spin−orbit coupling is strong, i.e., $k_BT \ll \zeta$ ($y \ll 1$). In this case, the square of the effective magneton number n_{eff}^2 is proportional to the temperature T (Figure 6) according to

$$n_{\text{eff}}^2 \approx 36y = 72 \cdot \frac{k_BT}{\zeta}.$$

Since the magnetic susceptibility is given by

$$\chi_{\text{mole}} = \frac{N_L^2\mu_0\mu_B^2 n_{\text{eff}}^2}{3RT}$$

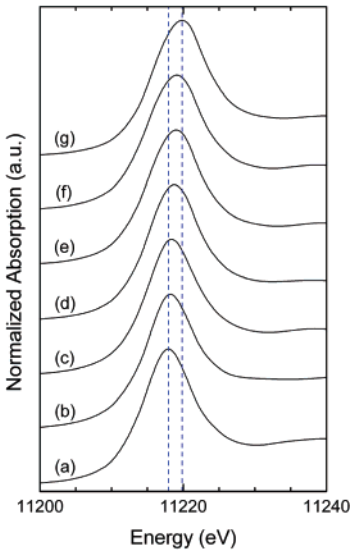

Figure 7. Normalized Ir-L_{III} edge XANES spectra for (a) $La_2ZnIr^{IV}O_6$, (b) $Ir^{IV}O_2$, (c) $Sr_2Ir^{IV}O_4$, (d) $Sr_2FeIr^{V}O_6$, (e) $Sr_2YIr^{V}O_6$, (f) $La_{1.2}Sr_{2.7}IrO_{7.33}$, and (g) $Sr_2CaIr^{VI}O_6$. The two dashed lines illustrate the white line shift to higher energies with increasing oxidation state of iridium.

it follows that the magnetic susceptibility χ is independent of T. The experimentally observed dependence of n_{eff}^2 on temperature for $La_{1.2}Sr_{2.7}IrO_{7.33}$ is illustrated in Figure 6. Data were fitted with a linear regression according to

$$n_{\text{eff}}^2 = A + BT$$

with $A = 0.0159(3)$ and $B = 0.005921(2)$. The very small value for A strongly indicates that nearly all iridium ions are in the oxidation state +5, based on the fact that the magnetic susceptibility for Ir^{6+} (ground term $^4A_{2g}$) and Ir^{4+} (ground term $^2T_{2g}$) ions would follow a Curie−Weiss law. The spin−orbit coupling constant ζ can be calculated from the equations above to be ∼8450 cm^{-1}. This value is in good agreement with results reported in earlier publications,[23,25,26] where ζ is in the range 5000−9000 cm^{-1}.

XANES Measurements. The above-mentioned results already show that the oxidation state of iridium in $La_{1.2}Sr_{2.7}IrO_{7.33}$ is +5. Nevertheless, we were looking for a more direct method to investigate the electronic structure of the transition metal. For this reason, XANES studies have been systematically carried out at the Ir-L_{III} edge for a series of compounds, namely La_2ZnIrO_6, IrO_2, Sr_2IrO_4, Sr_2FeIrO_6, Sr_2YIrO_6, and Sr_2CaIrO_6. In these oxides, the iridium ions are stabilized in an octahedral oxygen environment with the oxidation states +4 (d^5), +5 (d^4), and +6 (d^3). For $La_{1.2}Sr_{2.7}RuO_{7.33}$, similar measurements at the ruthenium L_{III}-absorption edge were carried out. The results proved that Ru is in the oxidation state +5. Details of these investigations can be found in ref 15. Figure 7 presents normalized Ir-L_{III} edge XANES spectra for the studied perovskite and the

(23) Jørgensen, C. K.; Owen, J.; Griffith, J. S.; Figgis, B.; Williams, R. J. P.; Orgel, L. E.; Rossotti, F. J. C.; Englman, R.; Sharp, D. W. A.; Magnusson, E. A.; Brown, M. G.; Chatt, J.; Prue, J. E.; Staveley, L. A. K.; Sharpe, A. G. *Discuss. Faraday Soc.* **1958**, *26*, 172.
(24) Kotani, M. *J. Phys. Soc. Jpn.* **1949**, *4*, 293.
(25) Hayashi, K.; Demazeau, G.; Pouchard, M.; Hagenmuller, P. *Mater. Res. Bull.* **1980**, *15*, 461.
(26) Wakeshima, M.; Harada, D.; Hinatsu, Y. *J. Alloys Compd.* **1999**, *287*, 130.

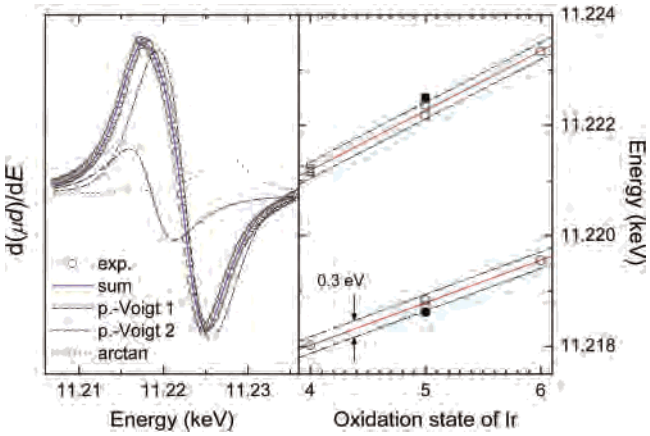

Figure 8. Left: Fit of the first derivative of the Ir-L_{III} XANES data for $La_{1.2}Sr_{2.7}IrO_{7.33}$ using two pseudo-Voigt and one arctangent functions. Right: Plots of the energy position corresponding to transitions to t_{2g} (○) and e_g (□) states versus the oxidation state of iridium in the studied compounds. Solid lines represent linear fits for the reference materials; solid symbols represent the energy values for $La_{1.2}Sr_{2.7}IrO_{7.33}$.

reference compounds. For all samples, a pronounced white line corresponding to transitions of 2p core electrons to unoccupied bound states with predominantly d character can be observed. It has been generally accepted to analyze these edge spectral features by fitting them with a combination of two pseudo-Voigt and one arctangent functions. These functions represent transitions to bound states and to the continuum, respectively. To improve the resolution, the first or second derivatives of the spectra are usually used. If the second derivative is fitted, the contribution of the arctangent becomes so small that it can well be neglected.[27−29] For ruthenium-containing perovskite oxides, there is a clear splitting of the white line into two peaks assigned to transitions to t_{2g} and e_g states.[30−32] Due to the higher natural line width[33] and the lower instrumental resolution at higher energies, the iridium L_{III} XANES spectra exhibit only one broad feature rather than two independent peaks. To estimate peak positions more accurately, curve fitting was done using the first-derivative spectrum. The fit for the title compound $La_{1.2}Sr_{2.7}IrO_{7.33}$ is represented in Figure 8 (left). The obtained energy positions of both pseudo-Voigt functions are plotted versus the oxidation state of iridium in Figure 8 (right). For the reference samples $La_2ZnIr^{IV}O_6$, $Ir^{IV}O_2$, $Sr_2Ir^{IV}O_4$, $Sr_2FeIr^{V}O_6$, $Sr_2YIr^{V}O_6$, and $Sr_2CaIr^{VI}O_6$, a linear increase to higher energies with increasing oxidation state of iridium can be observed. It should be mentioned that for IrO_2 and Sr_2IrO_4 it was only possible to fit one instead of two pseudo-Voigt functions. The obtained energy values for $La_{1.2}Sr_{2.7}IrO_{7.33}$ are within an estimated accuracy of ±0.2 in good agreement with the oxidation state of +5. The average energy splitting between transitions to t_{2g} and e_g states increases from 3.17 eV for Ir^{4+} to 3.79 eV for Ir^{6+}, consistent with previous XANES studies on iridium-containing perovskites.[28,29] The comparatively large energy splitting of 3.88 eV for $La_{1.2}Sr_{2.7}IrO_{7.33}$ can be explained by significant changes in the covalent character of the Ir−O bonds.[29] In analogy to the investigated double perovskites A'_2AIrO_6 (A′ = La, Sr; A = Zn, Fe, Y, Ca), the Ir−O bond in the studied compound $(A'_2O_{1+\delta})(A_2IrO_6)$ (A = La/Sr; A′ = Sr) competes with the A′−O and A−O bonds by sharing the same oxygen 2p orbitals via a pathway of nearly 180° and 90°, respectively. The degree of covalency of the Ir−O bond is therefore altered by the ionicity/covalency of these competing bonds. For the latter, Pauling's ionicities, which are deduced from the electronegativities of the participating atoms, can be used as a measure. Comparing, for example, Sr_2FeIrO_6 and $La_{1.2}Sr_{2.7}IrO_{7.33}$, ionicities for the Fe−O and La/Sr−O bonds are 0.502 and 0.763/0.803, respectively. Due to the higher average ionicity of the A−O and A′−O bonds in $La_{1.2}Sr_{2.7}IrO_{7.33}$, the Ir−O bond covalency in the title compound is higher than that in Sr_2FeIrO_6. This enhanced Ir−O bond covalency in turn leads to a larger energy splitting of the t_{2g} and e_g states consistent with our results.

Conclusion

Solid-state synthesis was used to prepare the new compound, $La_{1.2}Sr_{2.7}IrO_{7.33}$, which is the third example for an $n = 2$ member of the $(A'_2O_{1+\delta})(A_nB_{n-1}O_{3n})$ family of hexagonal perovskite-related oxides. Both title compounds, $La_{1.2}Sr_{2.7}RuO_{7.33}$ and $La_{1.2}Sr_{2.7}IrO_{7.33}$, have the transition metal cations in a high oxidation state (+5) as confirmed by the temperature dependence of the magnetic susceptibility as well as by XANES investigations. In contrast to the ruthenate, which shows Curie−Weiss behavior with an antiferromagnetic transition at 7 K, the magnetic susceptibility of the iridate is almost temperature-independent and can be explained by a large spin−orbit coupling typical for 5d transition metals.

With regard to the oxygen stoichiometry, a δ value of about $^1/_3$ for both the ruthenate and the iridate was determined by joint Rietveld refinement of X-ray and neutron diffraction data. This finding strongly confirms a structural model with both oxide and peroxide ions within the $(A'_2O_{1+\delta})$ layers. As mentioned in the Introduction, the close packing of (AO_3) layers in perovskites normally does not allow the incorporation of complex anions. All structures of the $(A'_2O_{1+\delta})$-$(A_nB_{n-1}O_{3n})$ family, however, have large hexagonal cavities built by six triangular $A'O_6$ prisms. These large cavities apparently facilitate the storage of extra oxygen in the form of peroxide (O_2^{2-}) ions.

It is to be noted that all previously reported members of the $(A'_2O_{1+\delta})(A_nB_{n-1}O_{3n})$ hexagonal perovskites are either pure oxides ($\delta = 0$) or pure peroxides ($\delta = 1$). For the two title compounds, on the other hand, we found both oxide and peroxide ions within the intermediate layers. The

(27) Lytle, F. W.; Greegor, R. B. *Appl. Phys. Lett.* **1990**, *56*, 192.
(28) Choy, J.-H.; Kim, D.-K.; Demazeau, G.; Jung, D.-Y. *J. Phys. Chem.* **1994**, *98*, 6258.
(29) Choy, J.-H.; Kim, D.-K.; Hwang, S.-H.; Demazeau, G. *J. Am. Chem. Soc.* **1995**, *117*, 8557.
(30) Choy, J.-H.; Kim, J.-Y.; Hwang, S.-H.; Kim, S.-J.; Demazeau, G. *Int. J. Inorg. Mater.* **2000**, *2*, 61.
(31) Kim, J.-Y.; Hwang, S.-H.; Kim, S.-J.; Demazeau, G.; Choy, J.-H.; Shimada, H. *J. Synchrotron Radiat.* **2001**, *8*, 722.
(32) Ebbinghaus, S.; Hu, Z.; Reller, A. *J. Solid State Chem.* **2001**, *156*, 194.
(33) Krause, M. O.; Oliver, J. H. *J. Phys. Chem. Ref. Data* **1979**, *8*, 329.

determined O−O bond length of approximately 1.54 Å is typical for peroxide ions.

The observed δ value very close to $^1/_3$ led us to search for possible superstructure reflections, which might explain this specific value. Neither X-ray nor neutron diffraction revealed any hints for such reflections. Therefore, we conclude that there is no intrinsic reason for the observed δ value, and we assume that it is due to the preparation conditions chosen. To clarify this point, we are currently systematically modifying the synthesis temperature and oxygen pressure to study the effect on δ. First experiments indicate that the $n = 2$ phase already forms at 1000 °C with slightly enlarged cell parameters. Detailed results of these experiments will be reported soon.

Acknowledgment. This work is based on experiments performed at the Swiss spallation neutron source SINQ, Paul Scherrer Institute, Villigen, Switzerland. We also gratefully acknowledge the provision of beamtime and resources at HASYLAB. Financial support was received from the Deutsche Forschungsgemeinschaft within SFB 484 and from the EU via access programs.

IC050511S